JMEPEG (2020) 29:8013–8024
https://doi.org/10.1007/s11665-020-05254-2

1059-9495/$19.00

Wear Resistance under Different Temperatures of NiCr-Cr_3C_2 Coating Remelted by Tungsten Inert Gas Arc

Li Guo-lu, Yuan Jing-min, Dong Tian-shun, Zhao Xiang-wei, Fu Bin-guo, and Shi Jiadong

Submitted: 20 July 2020 / Revised: 24 September 2020 / Accepted: 18 October 2020 / Published online: 2 November 2020

In this work, a NiCr-Cr_3C_2 coating was prepared on the AISI 1045 steel substrate by plasma spraying, then subjected to tungsten inert gas arc (TIG) remelting treatment. The microstructure, hardness and the wear test under different temperatures (25, 200, 400, and 600 °C) of the NiCr-Cr_3C_2 coatings before and after remelting were studied comparatively. The results show that after TIG remelting, the internal structure of the coating was dense, and the defects were greatly reduced. The hardness of the remelted coating surface became uniform and increased from 1007 $HV_{0.1}$ to 1141 $HV_{0.1}$, with an increase of 13.3%. At different temperatures, the weight loss of the remelted coating was always less than that of the sprayed coating, with a significant reduction of about 75%. The friction coefficients of the remelted coating and sprayed coating at 25 and 200 °C were basically the same, while the friction coefficients of the remelted coating at 400 and 600 °C were smaller than that of the sprayed coating. The wear mechanism of the remelted coating under different temperature were abrasive wear and adhesive wear, while that of the sprayed coating were fatigue wear, abrasive wear, and adhesive wear. Therefore, the TIG remelting treatment can optimize the microstructure of the NiCr-Cr_3C_2 coating and remarkably improve the wear resistance.

Keywords high-temperature wear resistance, NiCr-Cr_3C_2 coating, plasma spraying, TIG remelting

1. Introduction

Chromium carbide is a commonly used thermal spraying material in engineering. There are three common Cr-C compounds, namely, Cr_3C_2, Cr_7C_3, and $Cr_{23}C_6$, whose hardness are quite high even at high temperatures (Ref 1-3). NiCr is a kind of commonly used alloy with excellent heat resistance and corrosion resistance (Ref 4). Thus, the coating prepared by NiCr-Cr_3C_2 has wonderful oxidation resistance and abrasion resistance even under severe conditions such as high temperature and heavy load. Its typical applications are boiler tube, metallurgical furnace roll, engine cylinder, etc., (Ref 5, 6).

A common process for preparing NiCr-Cr_3C_2 coating is plasma spraying (Ref 7). However, the coating prepared by this method is mechanically bonded to the substrate, and has many defects such as cracks, inclusions, and pores. This makes the coating easy to fail in practical applications, leading to the excellent properties of NiCr-Cr_3C_2 cannot be fully utilized (Ref 8, 9). Studies have shown that remelting the sprayed coating can optimize the microstructure and improve properties of the coating, and further extend the service life of the components (Ref 10-12). Tungsten inert gas arc (TIG) remelting has high processing temperature, concentrated energy, and its equipment cost is low which is beneficial for popularization (Ref 13-15). However, there are few reports on the research of using TIG remelting method to improve the performance of plasma-sprayed NiCr-Cr_3C_2 coating up to now. In particular, the effect of TIG remelting on the wear resistance of plasma-sprayed NiCr-Cr_3C_2 coating under different temperatures is unclear.

In this study, TIG process was used to remelt plasma-sprayed NiCr-Cr_3C_2 coating, aiming to study the wear resistance and wear mechanism of the remelted NiCr-Cr_3C_2 coating under different temperatures. This study has a reference value for improving the performance of NiCr-Cr_3C_2 coating and expanding its application.

Li Guo-lu, Yuan Jing-min, Dong Tian-shun, Zhao Xiang-wei, Fu Bin-guo, and **Shi Jiadong**, School of Materials Science and Engineering, Hebei University of Technology, Tianjin 300130, China. Contact e-mail: dongtianshun111@163.com.

2. Experimental Methods

2.1 Experimental Materials

In this work, AISI 1045 steel was selected as the substrate with a size of 60 mm × 30 mm × 10 mm. Coated NiCr-Cr_3C_2 composite powder was used, in which Cr_3C_2 was coated by NiCr. This structure can reduce the possibility of carbon loss during spraying (Ref 16, 17). The ratio of NiCr to Cr_3C_2 was 3:7, and composition of the powder was 19.38 C, 75.87 Cr, and 4.74 Ni (at.%). Particle size of the powder was 25-30 μm, and its morphology is shown in Fig. 1. The powder was spherical and porous, which was benefical to be heated evenly and had good fluidity in the spraying process.

2.2 Preparation of Coatings

The surface of the substrate was cleaned with acetone to remove oil, and sandblasted to improve the surface roughness before spraying. The BT-G3 plasma spraying system was used to prepare coating with a thickness of 300 μm. The sample was preheated before remelting, and it was held in a X-G01123 box-type furnace at 300 °C for 1 h. TIG remelting treatment was carried out by YC-300WX welding machine, and then the sample was placed in a furnace for heat preservation with 2 h at

300 °C. The parameters of plasma spraying and TIG remelting are shown in Table 1.

2.3 Coating Characterization and Performance Test

The Hitachi S4800 field emission scanning electron microscopy (SEM) was used to observe the microscopic morphology of the coatings, and the energy-dispersive spectroscopy (EDS) attached to the SEM was used for energy spectrum analysis. X-ray diffraction (XRD) model D/max/2500PC was used for phase analysis of powders and coatings. Tecnai F20 field emission transmission electron microscopy (TEM) was used to observe the crystal structure and high-resolution image of the coatings. HMV-2000 Vickers hardness tester was used to measure the hardness of the coatings. MG-2000 pin-disk wear tester was used to test the wear resistance of the coatings under different temperatures. The schematic diagram of the wear test is shown in Fig. 2. The material of the disk was AISI E52100 steel and its hardness is 58HRC. The test time was 20 min with a 400 N load and 200 r/min rotation. The test temperatures were 25 °C, 200 °C, 400 °C, and 600 °C, respectively. Before the test, the samples were kept in the furnace for 5 h at the corresponding temperature to make them completely oxidized, so as to avoid the influence of oxidation weight gain on the data of weight loss in the experiment.

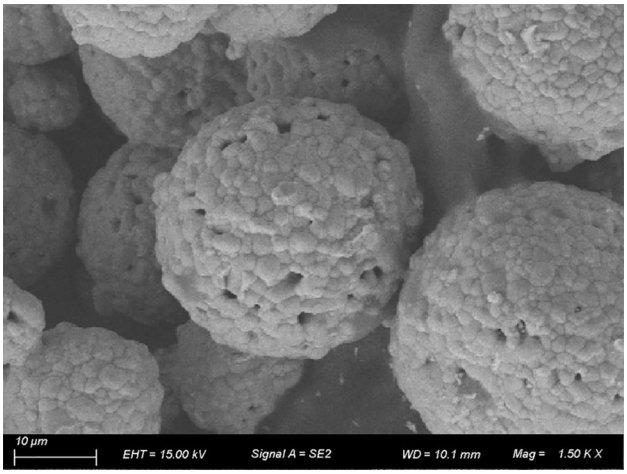

Fig. 1 Morphology of NiCr-Cr_3C_2 powder

Table 1 Parameters of plasma spraying and TIG remelting

Process	Parameters	Values
Plasma spraying	Cooling of substrate	Air blow
	Gas flow rate (L/min)	Ar(60), H_2(5)
	Spraying distance (mm)	110
	Voltage (V)	40
	Current (A)	800
	Coating thickness (μm)	300
TIG remelting	Argon flow (L/min)	10
	Arc length (mm)	2
	Current (A)	90
	Step size (mm)	1.5
	Scanning speed (mm/min)	200

3. Results and Discussion

3.1 Phase Analysis of the Coatings

The XRD patterns of the coatings are shown in Fig. 3. The main phases in the sprayed coating were Cr_3C_2, Cr_7C_3, $Cr_{23}C_6$ and Cr_3Ni_2. Cr_3C_2, Cr_7C_3 and $Cr_{23}C_6$ are high-quality ceramic phases (Ref 18, 19), whose existence will greatly improve the hardness of the coating. Diffraction peaks of Fe_3C and FeNi appeared in the diffraction spectrum of the remelted coating. The appearance of these two phases proved the occurrence of elements diffusion and the formation of metallurgical reactions between the coating and substrate. In addition, the diffraction peaks of Cr_3C_2 and Cr_7C_3 in the remelted coating decreased, while those of $Cr_{23}C_6$ increased, which was due to the carbon loss of Cr_3C_2 and Cr_7C_3 transforming into $Cr_{23}C_6$.

3.2 Morphology and Microstructure of the Coatings

The surface morphology of the sprayed coating is shown in Fig. 4(a). It can be seen that the surface of the sprayed coating was rough, with many defects such as cracks and pores. The

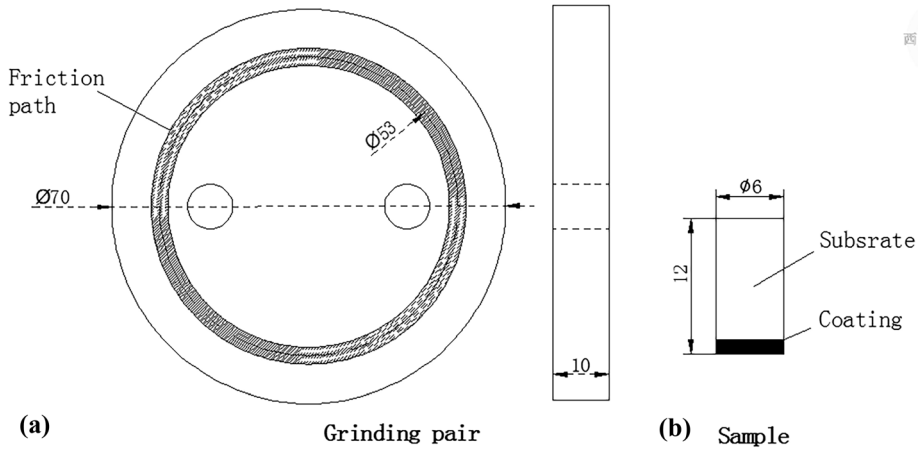

Fig. 2 Schematic diagram of grinding pair and sample

section morphology of the sprayed coating is shown in Fig. 4(b), illustrating the layered structure inside the sprayed coating. The interface between the sprayed coating and the substrate was serrated with poor bonding, which was a typical mechanical one (Ref 20). In addition, light gray phase (A) and dark gray phase (B) can be observed in the sprayed coating.

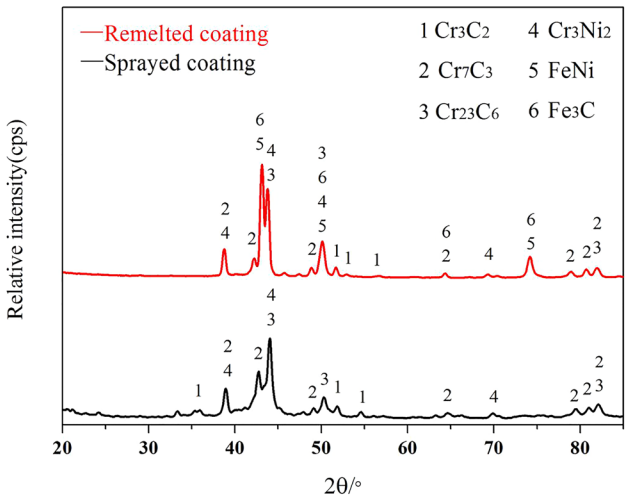

Fig. 3 XRD diffraction spectra of coatings

Figure 4(c) and (d) were EDS analysis results, which showed that region A was rich in Ni and region B was rich in Cr. Combined with the results of XRD analysis, it can be determined that the main phase in region A was Cr_3Ni_2, and the main phases in region B were chromium carbide, including Cr_3C_2, Cr_7C_3 and $Cr_{23}C_6$.

The surface morphology of the remelted coating is shown in Fig. 5(a). Compared with the sprayed coating, the surface of the remelted coating was relatively flat with fewer defects. The section morphology of the remelted coating in Fig. 5(b) showed that the interface between the coating and the substrate was smooth and neat, the width was about 10 μm, which was the characteristic of metallurgical bonding. So the bonding strength of the interface will be significantly improved (Ref 21-23). Besides, the internal structure of the remelted coating was dense, with few defects and obvious dendritic structure. EDS analysis of region C and region D are shown in Fig. 5(c) and (d), respectively. Combined with the results of XRD analysis, the main phase at the dendrite gaps was chromium carbide, while those in the dendrite were Fe_3C and FeNi.

The TEM morphology of the sprayed coating is shown in Fig. 6(a). Its microstructure can be divided into four regions: A, B, $C_{,1}$ and C_1'. Combining the EDS analysis of the region A with the XRD analysis of the sprayed coating, the main phase was determined to be Cr_3Ni_2. The electron diffraction patterns of region C_1 and C_1' are shown in Fig. 6(c) and (d). By measuring and calculating the crystal plane spacing, and

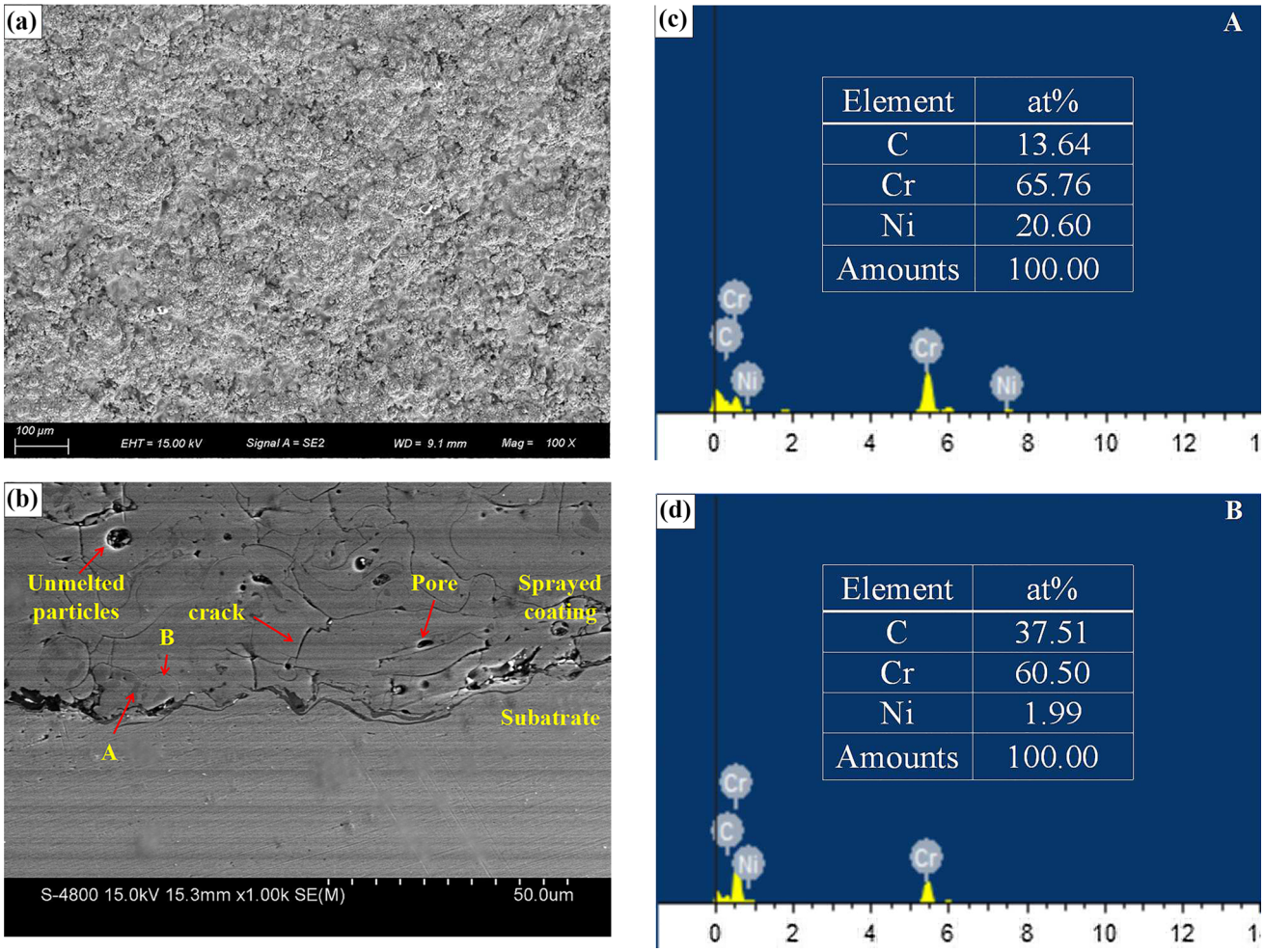

Fig. 4 Sprayed coating: (a) surface morphology; (b) section morphology; (c) EDS analysis of region A; (d) EDS analysis of region B

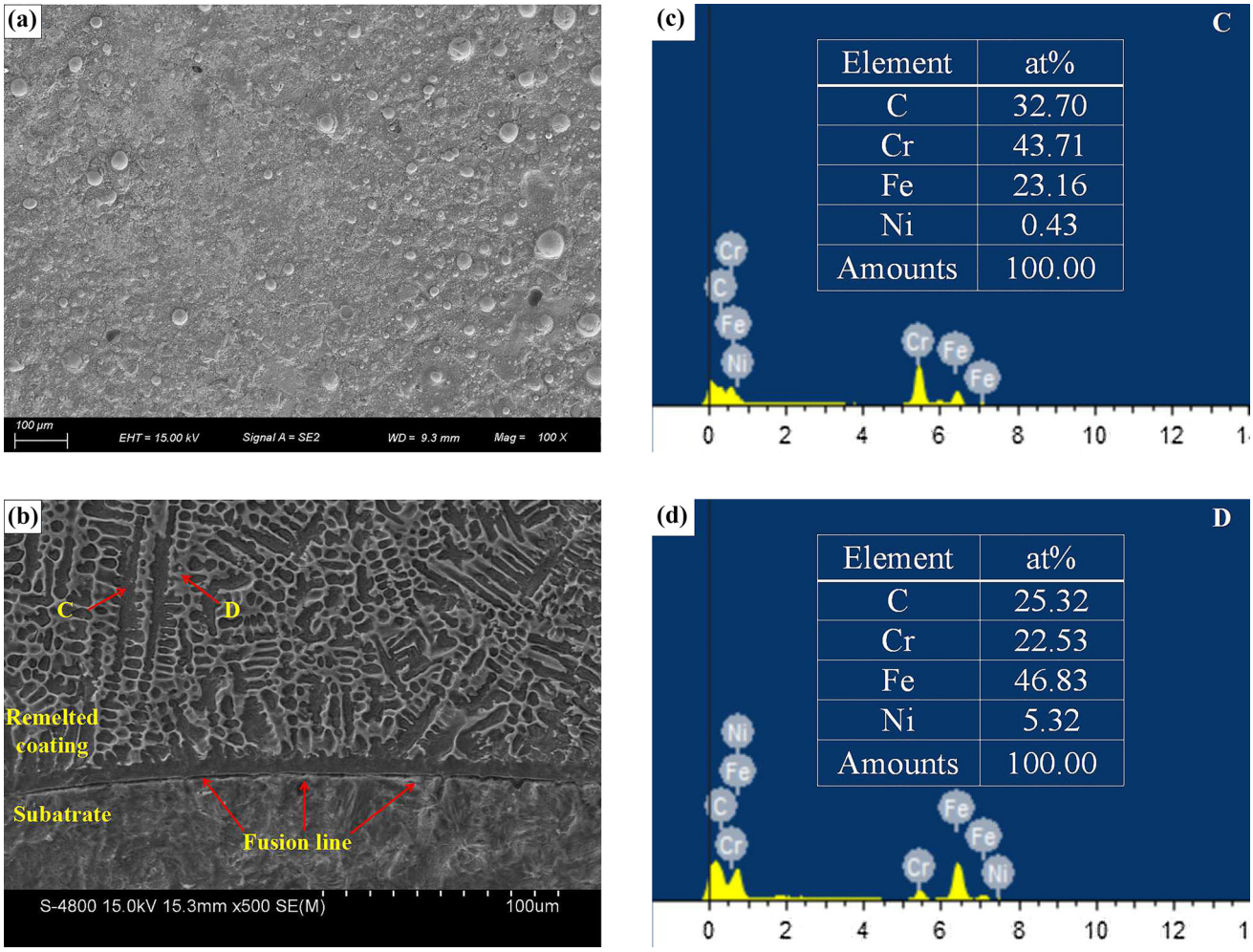

Fig. 5 Remelted coating: (a) surface morphology; (b) section morphology; (c) EDS analysis of region C; (d) EDS analysis of region D

comparing with the PDF card (38-0804, 36-1482), the main phases were determined to be Cr_3C_2 and Cr_7C_3, respectively. Region B belonged to the mixed crystal part of Cr_3Ni_2 and Cr_3C_2.

The TEM morphology of the remelted coating is shown in Fig. 7(a), which comprised three regions, i.e., D, $C_{,2}$ and C_2'. Based on EDS analysis of region D and XRD analysis of the remelted coating, the main phase was determined to be FeNi. The electron diffraction patterns of region C_2 and C_2 ‘ are shown in Fig. 7(c) and (d). By measuring and calculating the crystal plane spacing, and comparing with the PDF card (36-1482, 35-0783), the main phases were determined to be Cr_7C_3 and $Cr_{23}C_6$, respectively. This was because Cr_3C_2 and Cr_7C_3undergone a carbon loss reaction during remelting to produce $Cr_{23}C_6$.

In Fig. 7(a), according to rough measurement, the area of region C_2 was about 4 μm^2, and the area of region C_2' was about 0.4 μm^2. It can be found that the region C_2 was relatively thick, while the region C_2' was relatively tiny and evenly distributed. As a hard phase, tiny $Cr_{23}C_6$ was evenly dispersed in the coating by the form of particles. Such a tiny structure could hinder the movement of dislocations, thereby, achieving the effect of dispersion strengthening. This was very beneficial to the homogenization of the hardness distribution and the improvement in the hardness and wear resistance of the coating.

3.3 Hardness of the Coatings

Figure 8 shows the comparison diagram of the surface hardness of the sprayed coating and the remelted coating. The average hardness of them were 1007 $HV_{0.1}$ and 1141 $HV_{0.1}$, respectively, and the original data are shown in the Table 2. It indicates the remelted coating was slightly harder than the sprayed coating. Moreover, the hardness error value of the remelted coating(51 $HV_{0.1}$) was obviously lower than that of the sprayed coating(388 $HV_{0.1}$). This was due to the existence of defects such as pores and cracks in the sprayed coating led to the looseness of the structure and weak adhesion between the phases. While, the microstructure of the remelted coating was dense, moreover, tiny $Cr_{23}C_6$ distributed dispersively in the coating to play a strengthening role. Therefore, the hardness increased and its distribution became uniform.

3.4 Wear Resistance of the Coatings at Different Temperatures

3.4.1 Wear Resistance. The friction coefficients(FC) and weight loss(WL) of the coatings at different temperatures are shown in Table 3. The FC refers to the average value after the coefficient reached a stable value until the end of the test. It can be seen that at four temperatures, the wear loss of the remelted

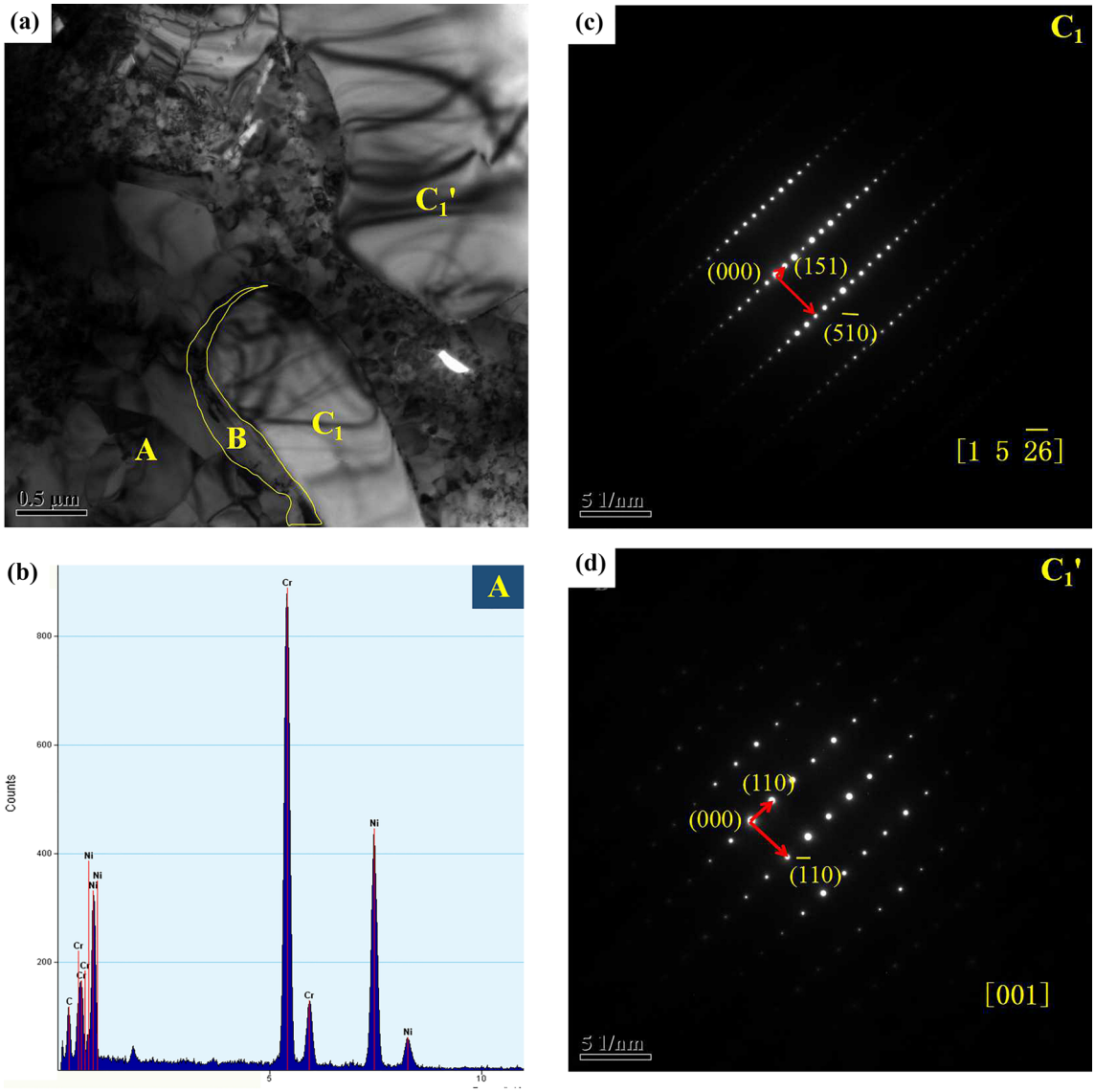

Fig. 6 Sprayed coating: (a) TEM morphology; (b) EDS analysis in region A; (c) diffraction pattern in region C_1; (d) diffraction pattern in region C_1'

coating is significantly less than that of the sprayed coating, and the former is only 25% of the latter. The friction coefficients of the remelted coating at 25 °C and 200 °C are basically the same as that of the sprayed coating, while the friction coefficients of the remelted coating at 400 °C and 600 °C are smaller than that of the sprayed coating.

3.4.2 Wear Mechanism. (1) Wear Mechanism at 25 °C

The wear scar morphologies of the coatings at 25 °C are shown in Fig. 9. There were pits and furrows on the wear scars of the sprayed coating. Pit was the characteristic of fatigue wear. While, there were furrows and oxide films on the wear scars of the remelted coating. EDS analysis was conducted on the oxide film (A) in Fig. 9(b). As shown in Fig. 9(c), the oxide film was rich in iron and oxygen, indicating the main component was iron oxide. Therefore, the wear mechanism of the sprayed coating was fatigue wear and abrasive wear, while that of the remelted coating was abrasive wear.

The formation mechanism of the pits on the sprayed coating can be illustrated in Fig. 10. There were many cracks inside the layer structure of the sprayed coating. Under the extrusion pressure and shear force of the grinding pair, the cracks expanded, and the surface material peeled off the coating, leaving pits. The remelted coating was dense with few defects, and its internal structure was not layered, so no pits formed, which means that no fatigue wear occurred. In the wear test of remelted coating, wear debris on the grinding ball fell after oxidation and stuck to the surface of the coating, thus forming an oxide film on the coating surface. Oxide film played a role of lubrication in the process of friction (Ref 24), so wear is reduced.

the oxide film in the wear scar of the remelted coating played a role of lubrication in the process of friction, so, wear is reduced.

(2) Wear Mechanism at 200 °C

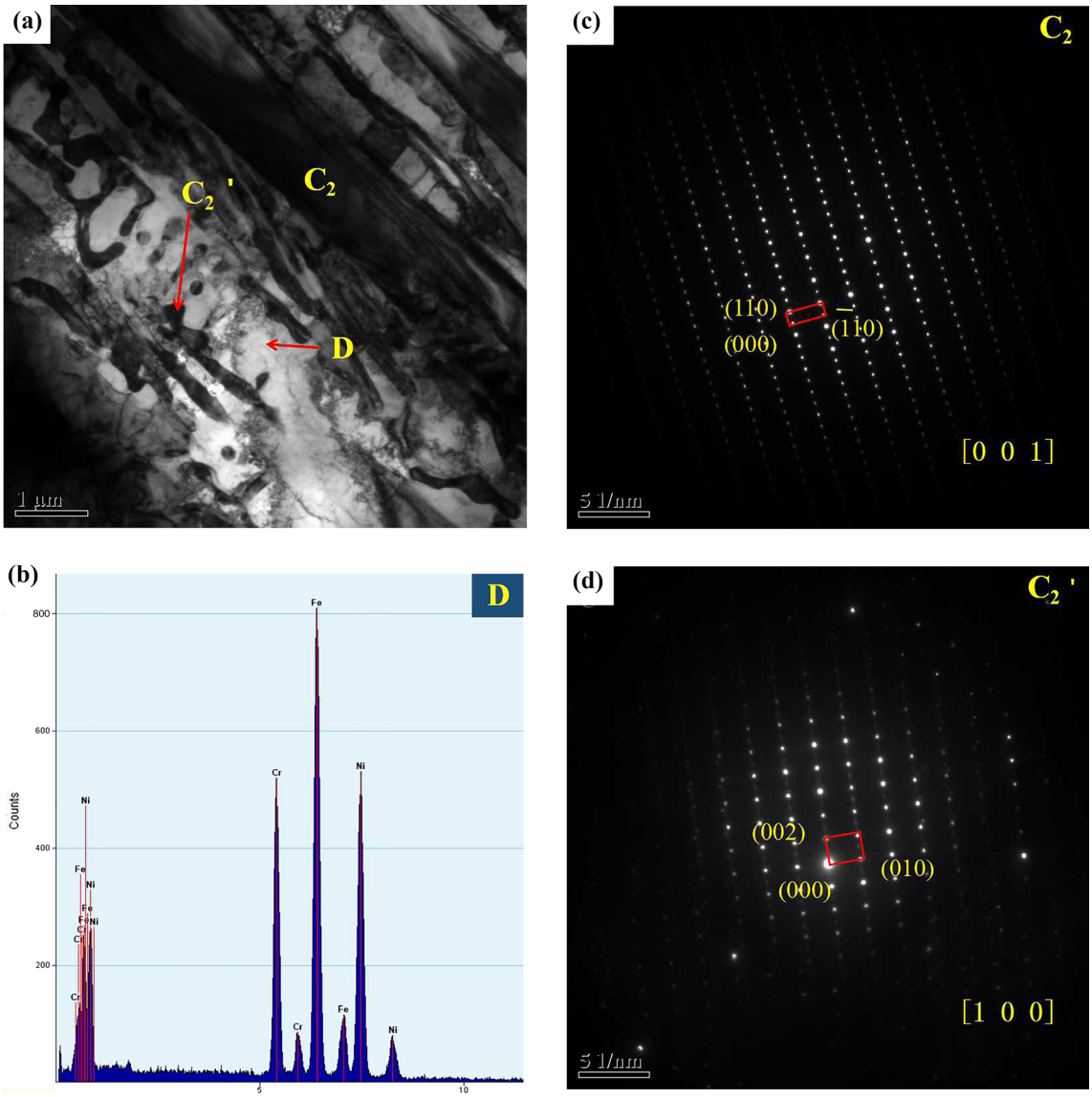

Fig. 7 Remelted coating: (a) TEM morphology; (b) EDS analysis in region D; (c) diffraction pattern in region C_2; (d) diffraction pattern in region C_2'

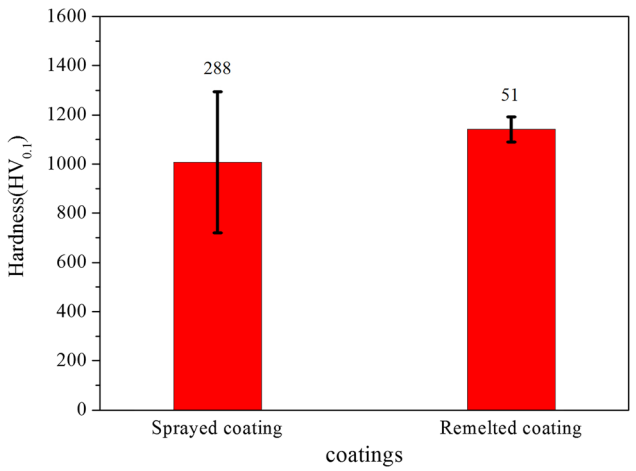

Fig. 8 Comparison of hardness between sprayed coating and remelted coating

The wear scar morphologies of the coatings at 200 °C are shown in Fig. 11. There were delamination and adhesion marks in the wear scars of the sprayed coating. Delamination was also the characteristic of fatigue wear. While, furrows and oxide films can be found in the wear scar of the remelted coating. Therefore, the wear mechanism of the sprayed coating were fatigue wear and adhesive wear, while that of the remelted coating was abrasive wear.

The formation mechanism of delamination on the sprayed coating at 200 °C can be illustrated in Fig. 12. At 200 °C, the ductility of the the sprayed coating was increased. Hence, the material of surface-layer plastically was pressed into a flaky shape by the grinding pair. As the wear progressed, the material of surface layer was squeezed and cracked under the combined force of friction shear force and extrusion force. The crack then propagated, causing the surface material to detached from the sprayed coating. The remelted coating was dense, and its internal structure was not layered, so no delamination formed, and the area of the oxide film reduced the wear.

Table 2 Surface hardness of the coatings

Number	1	2	3	4	5	6	7	8	9	10	11	12
Sprayed	1203	1081	1696	628	1039	823	1238	1051	634	1078	715	897
Remelted	1178	1191	1167	1169	1182	1149	1198	1112	1152	1101	1063	1031

Table 3 Friction coefficients(FC) and weight loss(WL) (10^{-3} mg)of the coatings at different temperatures

	25 °C		200 °C		400 °C		600 °C	
Temperature	FC	WL	FC	WL	FC	WL	FC	WL
Sprayed	0.34	18.9	0.35	16.4	0.39	5.9	0.41	7.5
Remelted	0.36	4.5	0.35	4.4	0.31	1.5	0.31	1.7

(3) Wear Mechanism at 400 °C

The wear scar morphologies of the coatings at 400 °C are shown in Fig. 13. The surface of the wear scars were wavy, and there were traces of adhesion. The phenomenon of adhesion was serious in the sprayed coating, while that of remelted coating was relatively slight. EDS analysis of the wavy front end is shown in Fig. 13(c) and (d), indicating its main component was iron oxide. At 400 °C, plastic deformation and adhesive wear occurred in both sprayed coating and remelted coating.

The wear mechanism of the coatings at 400 °C is shown in Fig. 14. Although the surface of the coating was carefully polished, it was still uneven at the micro-level. The plastic deformation capacity of the coating was improved at 400 °C. During the wear process, the surface of the coating presented wavy plastic deformation along the sliding direction due to the squeezing and shearing forces of the grinding pair. The front end of the wave after plastic deformation was tightly attached to the grinding pair. When it was hardly to withstand the shearing force, it would detach from the coating, causing adhesive wear. The front end of some waves was not easily detached from the coating. But, the surface material of the grinding pair in contact with the wave was sheared off and transferred to the coating surface, thereby, forming iron oxide film on the surface of the coating. Compared with the sprayed coating, the remelted coating had a dense internal structure, and the bonding force between the phases would also increase, so it was not easy to cause adhesive wear. While there were more materials transferred from the friction pair, forming a large oxide film area, so the wear was slight.

(4) Wear Mechanism at 600 °C

The wear scar morphologies of the coatings at 600 °C are shown in Fig. 15. Furrows and abrasive grains were found in the wear scars of the sprayed coating and the remelted coating. In addition, iron oxide was also present, and EDS analysis shows that its main component was iron oxide. Therefore, the wear mechanisms of sprayed coating and remelted coating were both abrasive wear.

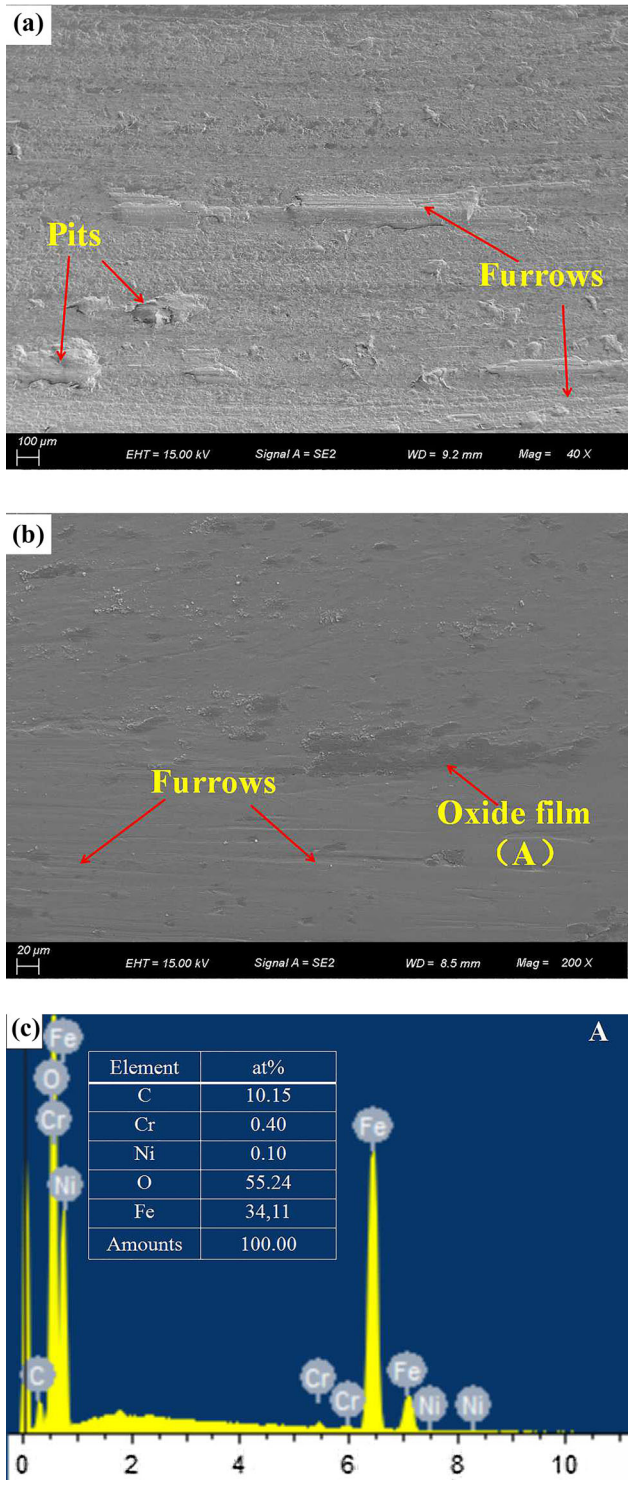

Fig. 9 Morphology of wear scars at 25 °C: (a) sprayed coating; (b) remelted coating; (c) EDS analysis of oxide film

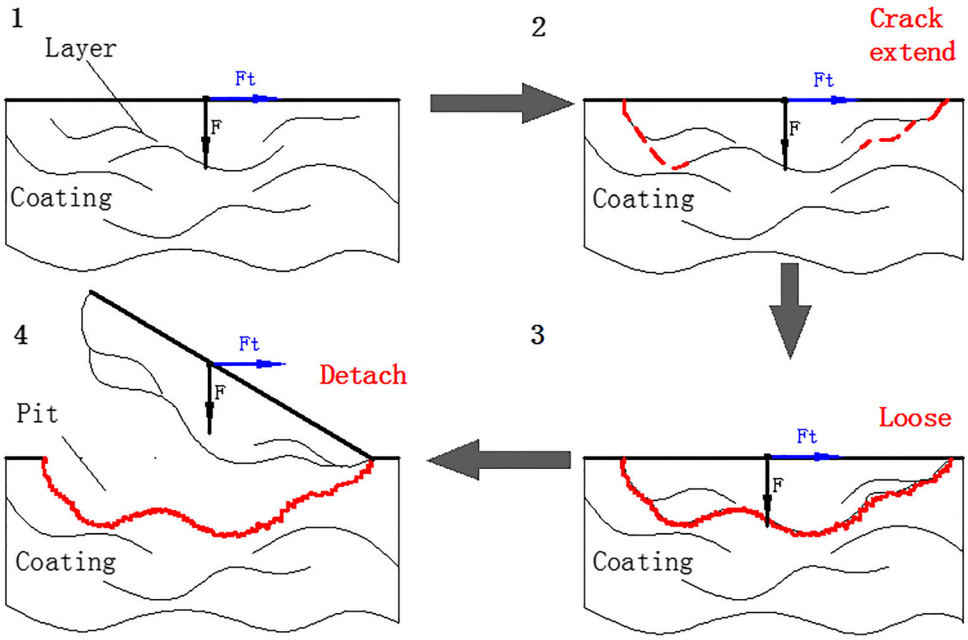

Fig. 10 Formation mechanism of the pits in the sprayed coating

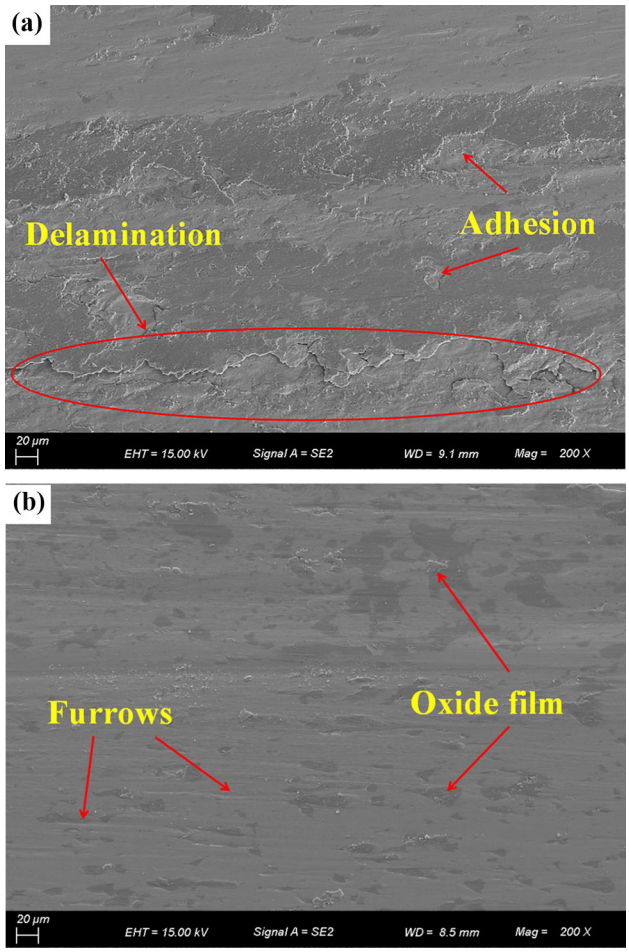

Fig. 11 Morphology of wear scars at 200 °C: (a) sprayed coating; (b) remelted coating

The wear mechanism of the coatings at 600 °C is shown in Fig. 16. At this temperature, the plastic deformation ability of the alloy phase was enhanced. While the ceramic phases have a stable structure. Even at 600 °C, they were still hard and the plastic deformation ability was still weak, which would cause a large hardness difference between the alloy phases and the carbide phases. The ceramic phases protruded from the surface of the coatings during the test and detached from the coatings under shearing force, and then they were used as abrasive grains between the coatings and the grinding pairs, resulting in abrasive wear. The ceramic phase particles in the sprayed coating were relatively large, and the furrows caused by abrasive grains were deep, resulting in serious wear. For the remelted coating, the main ceramic phase in the coating was $Cr_{23}C_6$, which was fine and dispersed, so the furrows caused by the abrasive grains were shallow. More importantly, the structure of Cr_3C_2 and Cr_7C_3 is orthogonal, and that of $Cr_{23}C_6$ is cubic. In comparison, the capacity of plastic deformation for $Cr_{23}C_6$ was relatively strong, so it was not easy to protrude from the coating. With the formation of FeNi alloy in the remelted coating, the bonding of the alloy phases to ceramic phases were enhanced. The ceramic phases did not easily detached from the coating, so the wear of the remelted coating was reduced.

According to the above wear test results, the wear resistance of the remelted coating is better than that of the sprayed coating at different temperatures. The reasons can be summarized as follows:

(1) In the process of wear, the loss of coating material was accompanied by the generation of cracks (Ref 25). The original pores or layered structure in the coating would accelerate the crack propagation, making the material easily detach from the coating. Compared with the sprayed coating, the remelted coating had less pores and the layered structure disappeared, so the wear resistance was improved.

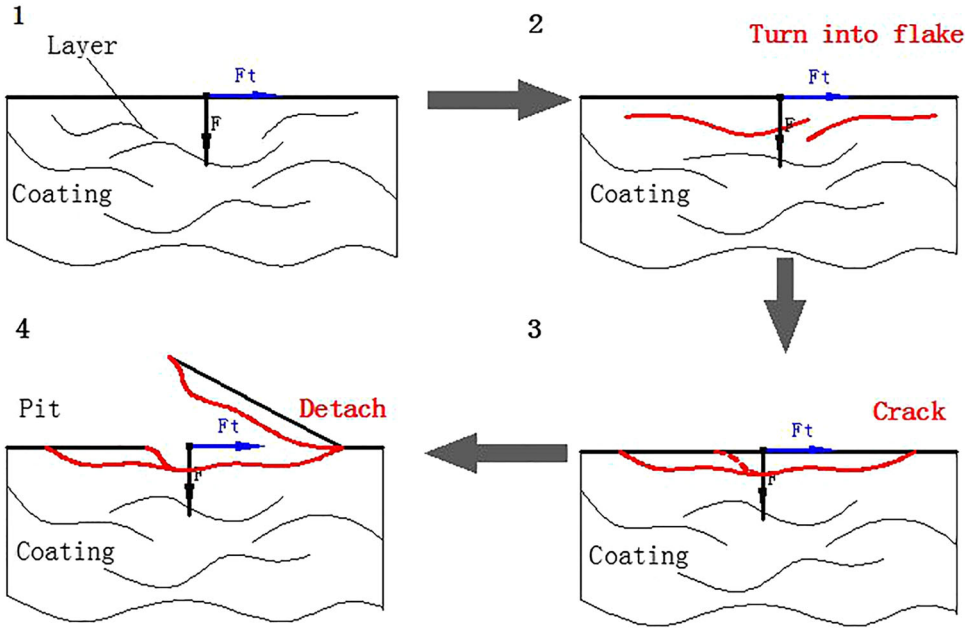

Fig. 12 Formation mechanism of delamination fracture in the sprayed coating

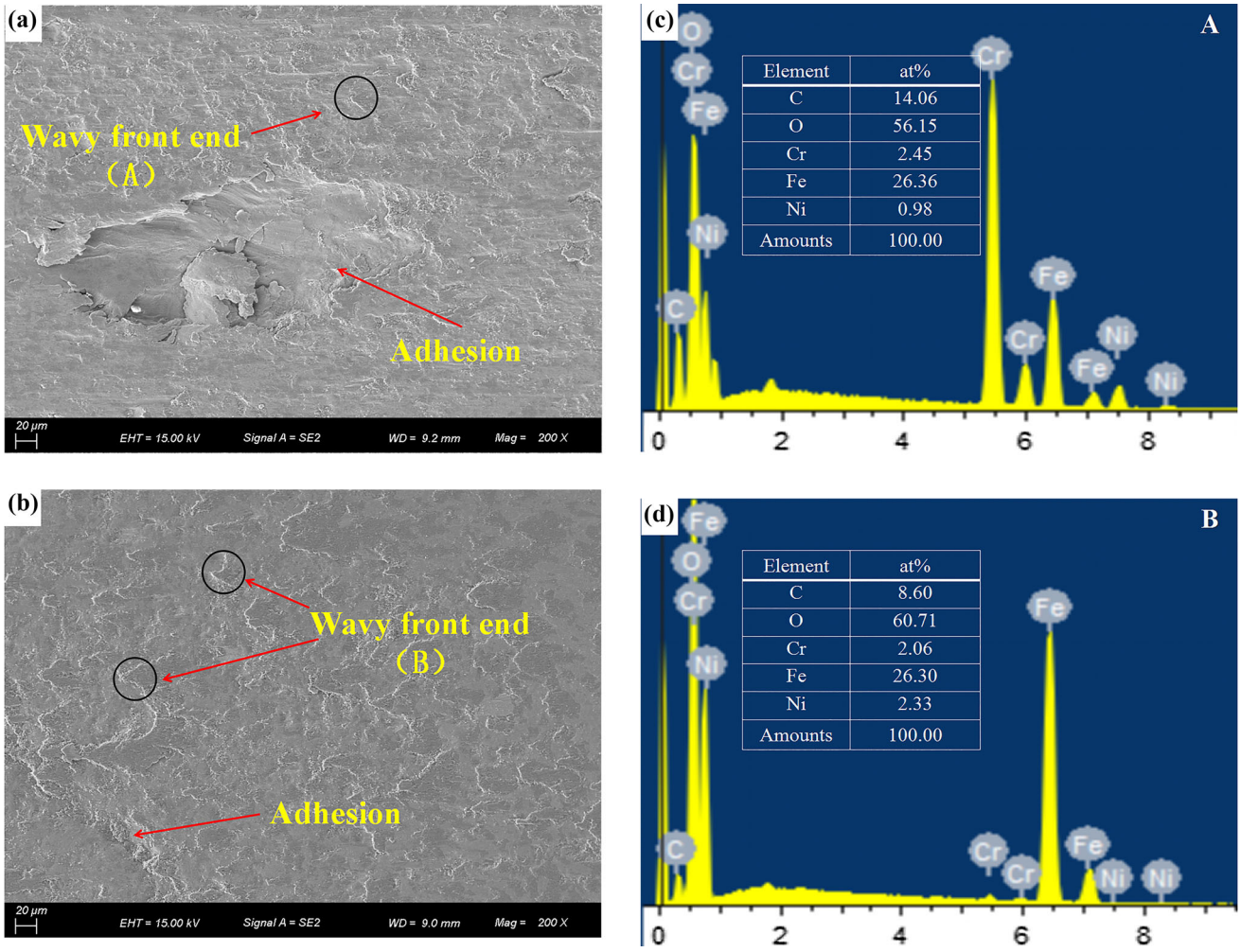

Fig. 13 Morphology of wear scars at 400 °C: (a) sprayed coating; (b) remelted coating; (c) EDS analysis of point A; (d) EDS analysis of point B

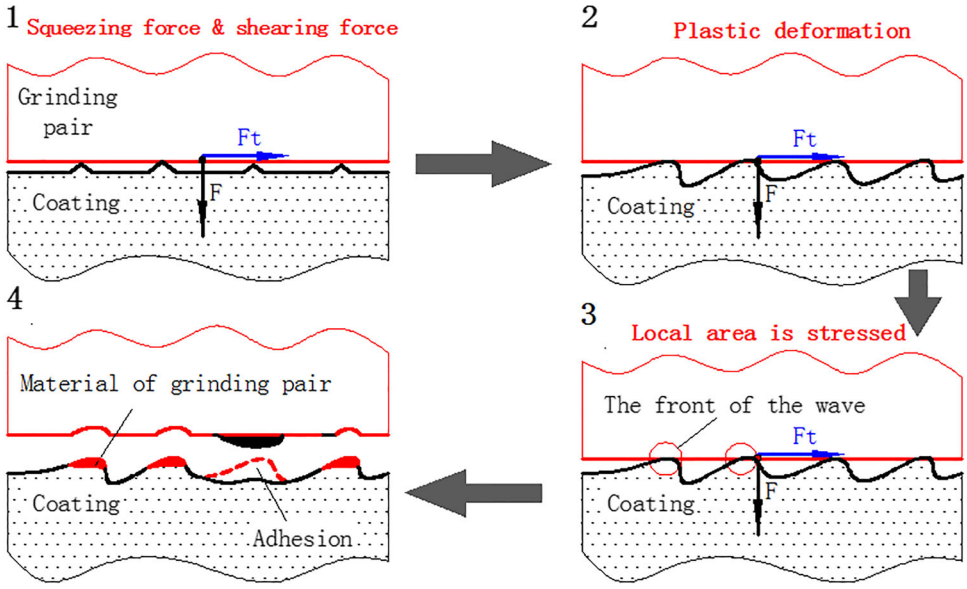

Fig. 14 Material loss mechanism of the coatings at 400 °C

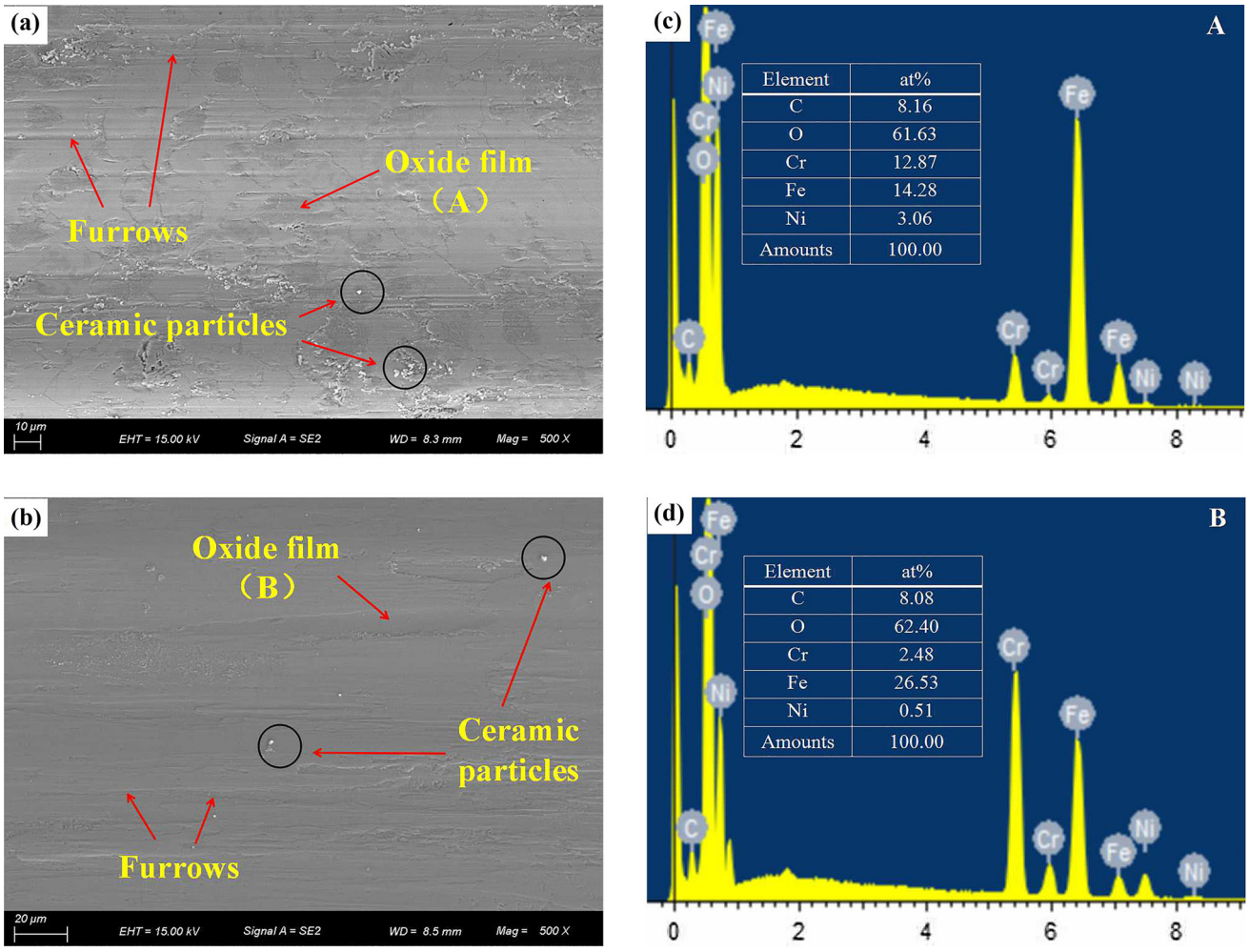

Fig. 15 Morphology of wear scars at 600 °C: (a) sprayed coating; (b) remelted coating. (c) EDS analysis of point A; (d) EDS analysis of point B

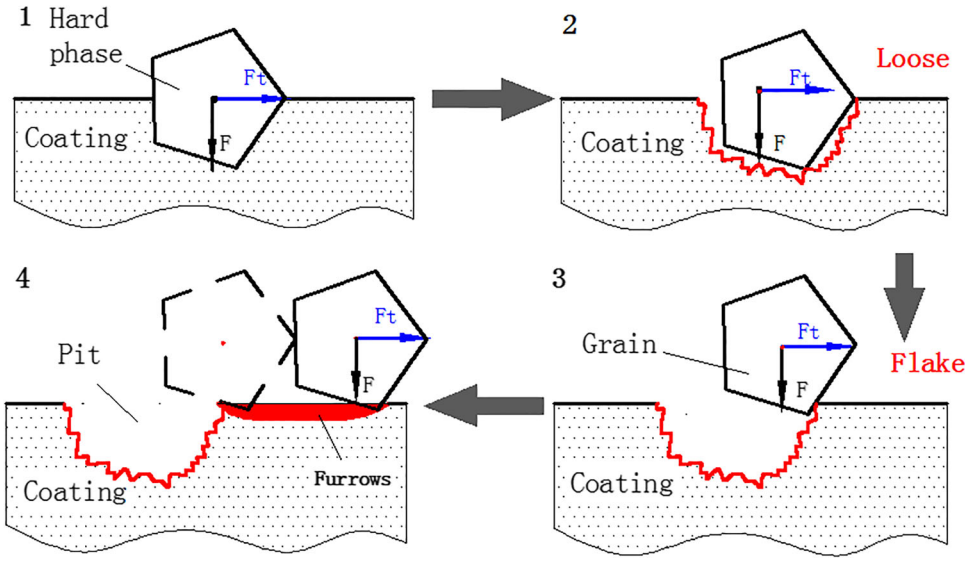

Fig. 16 Formation mechanism of abrasive wear in the coatings

(2) The ceramic phase in the remelted coating was finer. When the crack extended to the grain edge of the ceramic phase, the distance along the grain boundary of the ceramic phase was short. After entering the alloy phase, the crack propagation work was absorbed by the alloy phase through the plastic deformation capacity, the crack propagation was blocked and the material was not easy to fall off, so the wear resistance was improved.

(3) The wear resistance of the material was proportional to the hardness (Ref 26). The remelted coating was harder than the sprayed coating, and the hardness distribution was even, so the remelted coating had excellent wear resistance.

4. Conclusion

In this paper, a NiCr-Cr_3C_2 coating was prepared on AISI 1045 steel substrate by plasma spraying, and was remelted by TIG remelting process. On this basis, the effect of TIG remelting on the microstructure, mechanical properties, and wear resistance of the coatings at different temperatures was studied. The conclusions are as follows:

1. The sprayed NiCr-Cr_3C_2 coating had a layered structure with many defects, and the coating was mechanically bonded to the substrate. After TIG remelting treatment, the interior of the coating was dendrite structure with few defects, and there was a metallurgical bond between remelted coating and substrate. Hence, TIG remelting optimized the structure of the sprayed coating.
2. After TIG remelting, the carbon loss of Cr_3C_2 and Cr_7C_3 produced tiny and dispersed $Cr_{23}C_6$, whose dispersion strengthening effect increased the coating hardness from $1007HV_{0.1}$ to $1141HV_{0.1}$. In addition, the hardness distribution became uniform.
3. The wear resistance of the coatings at 25 °C, 200 °C, 400 °C, and 600 °C were studied, respectively. The weight loss of remelted coating was always less than that of sprayed coating, and the magnitude of reduction was about 75%. Therefore, TIG remelting significantly improved the wear resistance of sprayed NiCr-Cr_3C_2 coating.

References

1. L. Venkatesh, B. Venkataraman, M. Tak, G. Sivakumar, R.C. Gundakaram, and S.V. Joshi, Room Temperature and 600 °C Erosion Behaviour of Various Chromium Carbide Composite Coatings, *Wear*, 2019, **422–423**, p 44–53
2. T. Min, Y.M. Gao, Y.F. Li, Y. Ying, R.T. Li, and X.J. Xie, First-principles Study of the Tlectronic Structure, Hardness and Debye Temperature of Chromium Carbide, *Rare Metal Mat. Eng.*, 2012, **41**(02), p 87–91 (**in Chinese**)
3. R. Pileggi, M. Tului, D. Stocchi, and S. Lionetti, Tribo-corrosion Behaviour of Chromium Carbide Based Coatings Deposited by HVOF, *Surf. Coat. Technol.*, 2015, **268**, p 247–251
4. E.A. Lazareva, Heat-Resistant Sitall Coatings for High-Temperature Corrosion Protection of Nichrome Alloys, *Mater. Sci. Forum*, 2020, **992**, p 633–639
5. M. Mathapati, M. Doddamani, and M.R. Ramesh, High-Temperature Erosive Behavior of Plasma Sprayed Cr_3C_2-NiCr/Cenosphere Coating, *J. Mater. Eng. Perform.*, 2018, **27**(3), p 1–9
6. Q. Liu, T. He, W.Y. Guo, Y. Bai, Y.S. Ma, and Z.D. Chang, Tribological Behavior of SAPS Sprayed Al_2O_3-TiO_2 and NiCr-Cr_3C_2 Coatings under Severe Load Conditions, *Surf. Coat. Technol.*, 2019, **370**, p 362–373
7. S. Matthews, Development of High Carbide Dissolution/Low Carbon Loss Cr_3C_2-NiCr Coatings by Shrouded Plasma Spraying, *Surf. Coat. Technol.*, 2014, **258**, p 886–900
8. S. Xuanyu and Y. Suyuan, Performance in Resistance to Surface Fatigue for Cr_3C_2-25%NiCr Coatings by Plasma Spray and CDS Spray, *Tribol. Lett.*, 2004, **16**(3), p 173–180
9. E. Qin, B. Wang, W. Li, W. Ma, H. Lu, and S. Wu, Optimized Microstructure and Properties of Cr_3C_2-NiCr Cermet Coating by HVOF/Laser Hybrid Processing, *J. Therm. Spray Technol.*, 2019, **28**, p 1072–1080
10. K.A. Habib, D.L. Cano, C.T. Caudet, M.S. Damra, I. Cervera, and J. Bellés, Influence of Al_2O_3 Particle Size on Microstructure, Mechanical Properties and Abrasive Wear Behavior of Flame-Sprayed and

Remelted NiCrBSi Coatings, *J. Mater. Eng. Perform.*, 2017, **26**(4), p 1647–1656
11. R. Shoja, Reza, Laser Surface Treatment of Stellite 6 Coating Deposited by HVOF on 316L Alloy, *J. Mater. Eng. Perform.*, 2016, **25**(7), p 2583–2595
12. P. Hengst, R. Zenker, T. Süß, and K. Hoffmann, Improvement of the Load-bearing Capacity of Thermal Spray Coatings in Combination with Electron Beam Profiling and Electron Beam Remelt-bonding, *J. Heat Treat. Mater.*, 2016, **71**(6), p 265–271
13. T. Dong, X. Zheng, G. Li, H. Wang, M. Liu, and X. Zhou, Effect of Tungsten Inert Gas Remelting on Microstructure, Interface, and Wear Resistance of Fe-Based Coating, *J. Eng. Mater. Tech.*, 2018, **140**(4), p 0410071–0410078
14. K. Sudhir and P.K. Ghosh, TIG Arc Processing Improves Tensile and Fatigue Properties of Surface Modified of AISI, 4340 Steel, *Int. J. Fatigue*, 2018, **116**, p 306–316
15. S.C. Juang and Y.S. Tarng, Process Parameter Selection for Optimizing the Weld Pool Geometry in the Tungsten Inert Gas Welding of Stainless Steel, *J. Mater. Eng. Perform.*, 2002, **122**(1), p 33–37
16. V. Matikainen, H. Koivuluoto, P. Vuoristo, J. Schubert, and Š. Houdková, Effect of Nozzle Geometry on the Microstructure and Properties of HVAF-Sprayed WC-10Co4Cr and Cr_3C_2-25NiCr Coatings, *J. Therm. Spray Technol.*, 2018, **27**, p 680–694
17. Y. Li, X. Meng, R. Li, F. Zeng, and Y. Gu, Effect of Ni Content on Microstructure and Performance of Ni/Ceramic Composite Coating, *J. Mater. Eng. Perform.*, 2020, **29**(5), p 2853–2864
18. J.Y. Du, F.Y. Li, Y.L. Li, and L. Wang, Influences of Plasma Arc Remelting on Microstructure and Service Performance of Cr_3C_2-NiCr/NiCrAl Composite Coating, *Surf. Coat. Technol.*, 2019, **369**, p 16–30
19. F. Ye, Y. Xu, M. Hojamberdiev, Y. Lai, C. Wang, and X. Wang, Effect of Carbide Ceramic Zone on Wear Resistance of the (Fe, Cr)7C3/Fe Surface Gradient Composite, *J. Mater. Eng. Perform.*, 2015, **24**(8), p 2898–2907
20. G. Xie, Y. Lu, Z. He, B. Hu, and P. Lin, Microstructure and Corrosion Properties of Plasma-Sprayed NiCr–Cr_3C_2 Coatings Comparison with Different Post Treatment, *Surf. Coat. Technol.*, 2008, **202**(13), p 2885–2890
21. M. Arai, H. Ochiai, and T. Suidzu, A Novel Low-thermal-conductivity Plasma-sprayed Thermal Barrier Coating Controlled by Large Pores, *Surf. Coat. Technol.*, 2016, **285**, p 120–127
22. Z.Y. Piao, B.S. Xu, H.D. Wang, and D.H. Wang, Influence of Surface Nitriding Treatment on Rolling Contact Behavior of Fe-based Plasma Sprayed Coating, *Appl. Surf. Sci.*, 2013, **266**(1), p 420–425
23. J.B. Yu, Y. Wang, F.F. Zhou, and L. Wang, ZY Pan (2018) Laser Remelting of Plasma-sprayed Nanostructured Al_2O_3-20 wt.% ZrO_2 Coatings onto 316L Stainless Steel, *Appl. Surf. Sci.*, 2018, **431**(15), p 112–121
24. Z.X. Zhu, B.S. Xu, S.N. Ma, W. Zhang, and W.M. Liu, Friction Oxidation Behavior of High Velocity Arc Sprayed Fe-Al Coating in High Temperature Wear, *Chin. J. Mech. Eng.*, 2004, **40**(11), p 163–168 (**in Chinese**)
25. W. Wu, J. Liu, T. Hua, Z. Chen, J. Jiang, H. Wang, L. Liu, and X. Liu, Microstructure and Friction-Wear Behavior of Multi-arc Ion Plating TiAlNC Ceramic Coating on WC-6%Co Substrate, *J. Mater. Eng. Perform.*, 2018, **27**, p 4665–4671
26. D. Shu, Mechanical Properties of Engineering Materials, Mechanical Industry Press., 2016, p 88–127, (**in Chinese**)